Proceedings of IMECE'03
2003 ASME International Mechanical Engineering Congress & Exposition
Washington, D.C., November 16-21, 2003

IMECE2003-42823

MICROCOMBUSTORS BASED ON CONTROLLABLE SOLID FUEL ELEMENTS

Brian A. English/Georgia Institute of Technology

Heather H. DiBiaso/Georgia Institute of Technology

Mark G. Allen/Georgia Institute of Technology

ABSTRACT

This paper focuses on the control of solid-fuel burn rate by controlling the solid-fuel chemistry or by controlling heat losses. Laser cutting and lamination have been used to fabricate milli-scale test structures to characterize burn rates of composite solid fuel. The base ingredients for the solid fuels tested were phase-stabilized ammonium nitrate (PSAN), ammonium perchlorate (AP), and sodium azide (SA). These base ingredients were tested alone or mixed with hydroxyl-terminated poly-butadiene (HTPB) plus various accelerants.

Several experiments were performed to test the controllability of composite solid fuels. Burn-rate tests at atmospheric pressure consisted of 250 to 500 micron deep square combustion chambers packed with fuel and resistively heated on the top surface until combustion was achieved. Experiments were also performed to increase burn rate through chamber pressurization. Reaction times for a set amount of fuel were observed to increase exponentially as nozzle diameter was decreased. Finally, combustion chamber geometry was altered to control reaction propagation by increasing localized heat losses. A 500 micron thick triangular chamber was fabricated and ignited at the larger end, allowing the reaction to propagate toward the triangle tip. These results indicate that controllable actuation of solid propellants on the microscale for non-thrust, gas generation actuator applications is feasible.

INTRODUCTION

This paper focuses on the control of solid fuel burn rate by one of three means:

1- Changes in fuel composition;
2- Pressurization due to a nozzle;
3- Heat losses to the surroundings, or quenching.

The observations made can be used for the design of controllable fluidic microactuators for use in aerodynamic control applications. Such a device might be similar in design to current microthrusters without focusing on maximizing thrust or force impulse. Instead, thrust may be sacrificed for increased exhaust controllability.

Solid-fuel microrockets have been developed for kilogram-scale satellite control [1,2,3] and sensor platform deployment[4]. Teasdale[4] demonstrates the design and fabrication of mm-scale solid-propellant rockets for deployment of sensor platforms, also known as "Smart Dust." These microthrusters use an ammonium-perchlorate (AP) propellant, and integrate igniters and thermopiles into the nozzle assembly. This shows that moldable solid fuel may be integrated into a MEMS fabrication process. The total device height was 8.5 mm to compensate for thermal losses to the sidewalls, yet thrust-to-mass ratios of 15mN/g were reported.

Lewis et al.[1] and Rossi et al.[2,3] have demonstrated solid-fuel microthrusters for use in kilogram-scale satellite control. Both demonstrated integration of solid fuel with MEMS processing. Lewis fabricated an array of chambers for the combustion of lead styphnate that used a 3-layer bonding technique to integrated fuel, igniter, and a burst diaphragm into an array of microthrusters. Individual devices were 300 to 500

microns in diameter by 1.5 mm thick. Thrust was reported at 0.1 mN, and combustion was reported to be approximately 10% of the total fuel. Rossi also used a 3-layer bonding technique, but combusted Glycidyl-Azide-Polymer (GAP) to characterize nozzle performance. Thrust measurements for GAP-based microthrusters were reported to be 2.5 to 75 mN for 4mm diameter combustion chambers. Both Lewis and Rossi noted that microthrusters offer more accurate control than their larger counterparts and simplified fabrication compared to liquid microthrusters.

The microrocket research demonstrates that solid fuel is beneficial for several reasons. It offers a reliable means for generating accurate fluidic forces, and thrust-to-weight ratios exceed unity. Solid fuel greatly reduces the complexity of the fabrication for micro-combustors and simplifies integration with MEMS-fabricated electrical components. There are no external storage requirements with solid fuel because the fuel and oxidizer are bound by a plasticizer and stored in the combustion chamber until needed. However, microrocket research focuses on maximizing thrust or impulse performance, so quenching effects may be detrimental to the performance of such devices.

Controllable solid fuel elements are similar to microthrusters in several ways. Both employ a simplified fabrication sequence, requiring very few support elements. This is especially true when compared to liquid or gas-phase combustors. Solid fuel mixtures produce 2 to 3 moles of gas per mole of solid, and several solid fuels have been demonstrated to combust with MEMS igniters. Contrary to the microthrusters presented, controllable solid fuel elements are not governed by the same performance issues. For example, maximum thrust can be traded either for controllability, or for duration of burn, depending on the application.

A potential application of these solid fuel elements is to generate large-force, controllable fluidic microactuators. These devices operate by expelling a jet of fluid into an embedding flow, and leveraging the energy of that flow to produce aerodynamic effects far in excess of the original thrust of the actuator[5]. One approach to these devices is the chemical generation of high-pressure gas followed by expulsion of that gas to interact with the embedding flow. Unlike conventional microthrusters, the design of such a devices requires the control of solid fuel, and may require that reaction rate and temperature be traded for gas generation capability and reaction controllability.

There are two important performance characteristics for a controllable solid fuel element. First, burn rate determines the rate of gas production for a given solid fuel. Control of burn rate sets exhaust jet magnitude. Secondly, burn time must be controlled to set an actuator pulse frequency. There are several ways to control a solid fuel[6]:

1- The base ingredients and mixture ratios
2- Catalysts and additives
3- Physical effects, such as particle size and sidewalls
4- Operating conditions, such as pressure, temperature, heat losses, and convection rate
5- Steady vs. unsteady operation

Fuel composition, nozzle pressurization, and quenching effects will be studied in an effort to control the combustion of solid fuel. Burn rate experiments are performed at a predicted device thickness of less than 500 microns. Burn rates are measured for three common base fuels and these burn rates are increased by adding various catalysts and metal fuels. Linear burn rates were measured between 0.23 and 2.35 mm/s. Next, nozzles are added to increase burn rate by pressurizing the chamber during the combustion process. This test showed burn rates as high as 12.63 mm/s for a 0.5 mm diameter nozzle. Finally, triangular combustion chambers are patterned from alumina to test quenching effects in the more energetic solid fuels. Initial conditions for all tests are standard atmospheric, and unsteady operation is assumed in contrast to typical large scale burn rate testing. Quenching distances of approximately 212 microns were measured for AP-HTPB mixtures.

The results demonstrate that solid fuel actuators may be controlled by fuel mixture, nozzle design, and combustion chamber design. The mixture and nozzle design may be varied to control gas production rate, therefore controlling the output magnitude of a fluid actuator, and the combustion chamber itself may be design to terminate a solid fuel reaction.

NOMENCLATURE

a: Linear burn rate coefficient for pressure
AD: Ammonium Dichromate
AP: Ammonium Perchlorate
c: Linear burn rate coefficient for nozzle diameter
D: Nozzle diameter
GAP: Glycidyl Azide Polymer
HTPB: Hydroxyl-terminated poly-butadiene
m: Linear burn rate exponent for nozzle diameter
n: Linear burn rate exponent for pressure
P: Absolute pressure
PSAN: Phase Stabilized Ammonium Nitrate
r = Linear burn rate [mm/s]
SA: Sodium Azide

Table 1. Solid Fuel Formulations

Fuel Component	Wt%	Wt%	Wt%	Wt%	Wt%	Wt%
PSAN-based formulations						
PSAN	100	80	70	60	57	51
Binder	0	20	20	20	20	20
Mg	0	0	10	20	20	20
AD	0	0	0	0	3	9
AP-based formulations						
AP	80	77.5	70			
Binder	20	20	20			
Al	0	2.5	10			
SA-based formulations						
SA	100	80	70	60		
Binder	0	20	20	20		
KNO3	0	0	10	20		

EXPERIMENTAL METHODOLOGY

Solid Fuel Preparation

There are three components to a composite solid fuel: a base ingredient, a polymeric binder, and any additives. Solid fuels in this study were typically mixed in quantities of 2 to 3 grams by hand mixing. The polymeric binder was always the first ingredient added. Metal powders were always added second and coated with the polymeric binder. After metal powders were added and coated, other additives were stirred into the mixture. Next, the base fuel was added and mixed, and finally a curing agent was added and stirred into the mixture. Once the curing agent is added to the solid fuel, the rubberized propellant may be pressed into any combustion chambers for one or two hours or until hardening of the propellant begins. The target weight of curing agent added was 0.19 x (weight of binder)

Three base ingredients were tested: AP, PSAN, and SA. For AP mixtures, aluminum powder was used as an additive and HTPB or GAP were used as binders. For PSAN mixtures, AD and Mg were used as additives and HTPB or GAP were used as binders. For SA mixtures, KNO_3 was used as an additive, and HTPB or GAP were used as binders. Ratios of base-fuel:additive:binder were varied for all base fuels in order to study effects on burn rates. Table 1 summarizes mixture formulation variables.

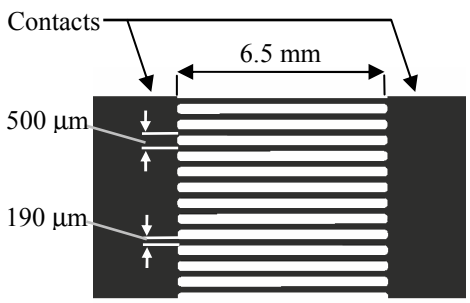

Figure 1. Titanium igniter for burn-rate experiments

Linear Burn Rate Testing

The purpose of these tests is to compare the linear burn rates of several fuel compositions under the same conditions. Linear burn rate test structures were designed to be approximately the size scale predicted for many future MEMS devices. Unlike large-scale solid-fuel testing, these linear burn-rate experiments measure average linear burn rates through a very short distance, approximately 200 to 500 microns, near the igniter during the initial, transient phase of the reaction. In these experiments and in later nozzle experiments, an average linear burn rate is reported by dividing the characteristic burn length by the total combustion time. Therefore, any reference to linear burn rate implies average linear burn rate calculated in the manner presented.

Tests were first completed using the non-energetic, HTPB binder with each of the base fuels. Then, additives were combined with the fuel mixtures and burn rates were compared. The fuel was ignited by hot-wire ignition, which applied a high heating rate on the top surface of the fuel. The top surface of the fuel was exposed to atmospheric pressure. An alumina test substrate, approximately 15 mm x 30 mm x 1 mm thick, was used to characterize the fuel. The combustion chamber was a 6.8 mm square, 500 microns deep. This depth of the combustion chamber was varied between 200 and 500 microns using 100 micron aluminum spacers. A titanium igniter, Fig. 1, was fabricated using 25.4 micron thick titanium shim stock and a 528 nm IR laser. The igniter consists of thirteen 190 micron wide wires, 6.5 mm long, and spaced 500 microns center-to-center. The melting temperature of titanium is 1670ºC.

With an igniter and combustion chamber prepared, solid fuel was pressed into the combustion chamber and an igniter was pressed onto the top surface. After curing for at least 12 hours, the burn rate test structure, Fig. 2(a) and 2(b), was ready to be tested. Ignition was achieved using a DC power supply and applying 30 W of DC power at 3.5 V. The high heating rate

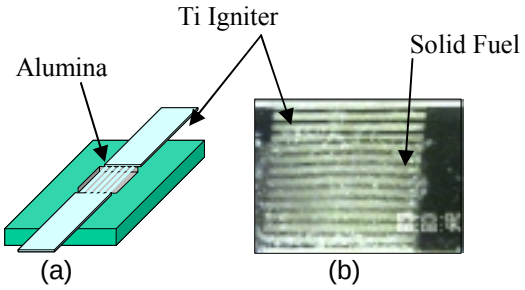

Figure 2. Burn-Rate Experimental Setup

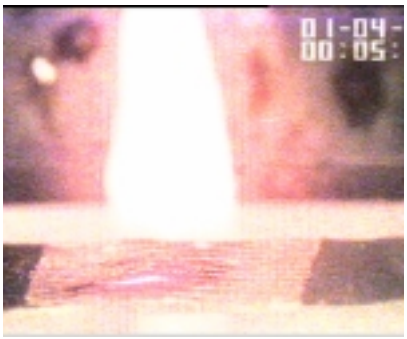

Figure 3. Burn-Rate Test

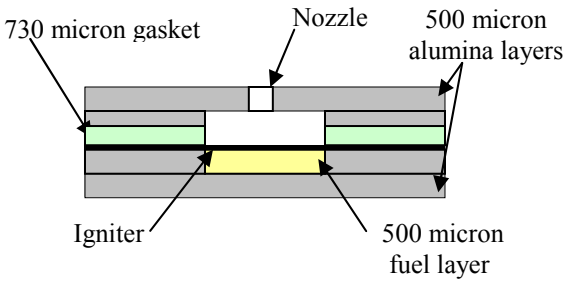

Figure 4. Sectional schematic of combustion chamber with nozzle

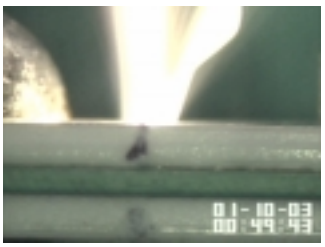

Figure 5. Nozzle burn-rate test with a 2 mm nozzle

was used to achieve ignition as quickly as possible and decrease unwanted heat conduction through the solid fuel.

Video timing was used to determine the burn time and burn rate was calculated by dividing the known fuel thickness by the burn time. The video system used consisted of a 3CCD camera and a capture card. The capture rate was limited to $1/15^{th}$ of a second. A burn-rate test may be seen in Fig. 3, where the timing display may be seen in the upper right corner. The test was performed at atmospheric pressure as a benchmark comparison for various solid-fuel compositions.

Linear Burn Rate Testing with Nozzle

To test effects of nozzle pressurization on linear burn rates, nozzles were added to the test structures described in Figures 2 (a) and (b). Theoretically, the linear burn rate of solid fuel is governed by Veille's Law:

$$r = aP^n$$

Veille's Law states that linear burn rate, r, is proportional to the pressure at the burning surface, P, to a power, n. Large-scale solid fuel testing typically uses a Crawford Bomb[7] to measure steady-state linear burn rates. The Crawford Bomb consists of velocity probes along the length of a strand of solid fuel contained within a variable pressure vessel. The experiments presented here are meant to compare pressurization-feedback effects on linear burn rates for solid fuel that is within 500 microns of the igniter. Not all formulations of solid fuel were tested; however, the results will depict a trend for using decreasing nozzle size to increase the linear burn rate of a solid fuel.

Cylindrical nozzles were laser cut into alumina substrates, where nozzle diameters are 0.5, 1, 2, or 3 mm. A region of air 1.25 mm thick was between the top surface of the fuel and bottom surface of the nozzle because a high temperature gasket was inserted between the combustion chamber and the exhaust nozzle. The solid fuel was heated by applying 30 W power at 3.5 V and measuring the combustion time using the video capture technique described before. Figure 4 depicts a sectional view of a typical combustion chamber with a nozzle and gasket attached. Figure 5 illustrates a typical experiment using a nozzle .

Quenching Test

Quenching tests were performed to test the propagation limits of the more energetic solid fuels, in particular, AP-based solid fuels. Knowing propagation limits

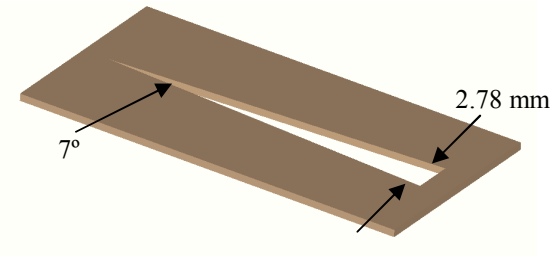

Figure 6. Quench Test Combustion Chamber

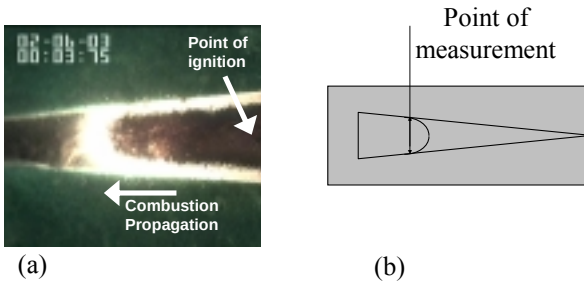

Figure 7. Quenching Test

allows for control of solid fuel by chamber design as well as solid-fuel composition and nozzle geometry.

Test structures were made from laser-cut alumina substrates, 250 to 1100 microns thick. The combustion chambers of the devices were in the shape of isosceles triangles as seen in Fig. 6. Solid fuel was packed into these devices in the same manner as the linear-burn-rate structures. Once the fuel had cured, an igniter was mounted on top of the larger end of the combustion chamber, and a 1 mm thick alumina substrate was placed over the remainder of the combustion chamber. A much smaller igniter was used for these tests as compared to the previous burn-rate experiments; the igniter was a single hot point approximately 250 microns wide. Once ignited, the combustion propagates towards the smaller end of the combustion chamber, and the combustion process terminates once heat losses to the alumina become too great to sustain the reaction. Figure 7 (a) is a still image of a quenching test in progress. The combustion front forms a meniscus as it travels along the length of the chamber. Once the combustion terminates, a measurement at the sides of the meniscus, see Figure 7 (b), was taken because that was determined to be the point where heat loss to the wall began dominating heat loss to the fuel. Taking the reciprocal of the surface-to-volume ratio at this point in the combustion chamber is the quenching distance.

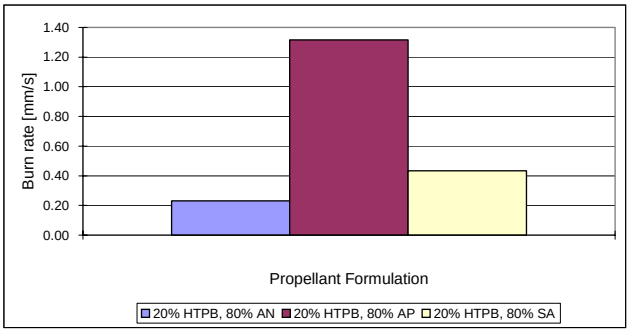

Figure 8. Average linear burn rates for base ingredients with non-energetic binder

RESULTS

Linear Burn Rate Testing

The first series of linear burn-rate experiments performed were to compare these base ingredients: AP, PSAN, and SA. As seen in Fig. 8, a base composition of 20% binder and 80% fuel, an AP-based fuel burns at a rate of 1.3 mm/s in the experiments described. This is approximately 3 times faster than SA-based fuels and 6 times faster than AN-based fuels.

AN-based Fuels. In the first series of experiments, Fig. 9, Fig. 10 and Table 2, AN-based fuel is loaded with various accelerants. Figure 9 shows that linear burn rates through 500 microns of fuel may be increased by adding Mg to the mixture. The burn rates are seen to increase from an average of 0.23 mm/s to 0.84 mm/s. The addition of a catalyst, AD, to a mixture of 20%Mg:20%HTPB/AN is seen to further increase the linear burn rate of AN-based solid fuels. The linear burn rate increases from 0.84 mm/s to 1.17 mm/s with the addition of 3% AD, and another slight increase to 1.23 mm/s with the addition of 9% AD. One final addition to the AN-based mixtures was the addition of an energetic binder, GAP. Table 2 presents results for the substitution of GAP for HTPB. The energetic GAP binder caused an increase of burn rate from 0.23 mm/s to 0.60 mm/s when used solely with AN; however, the linear burn rate increase was much less when metal fuels were mixed into the fuel.

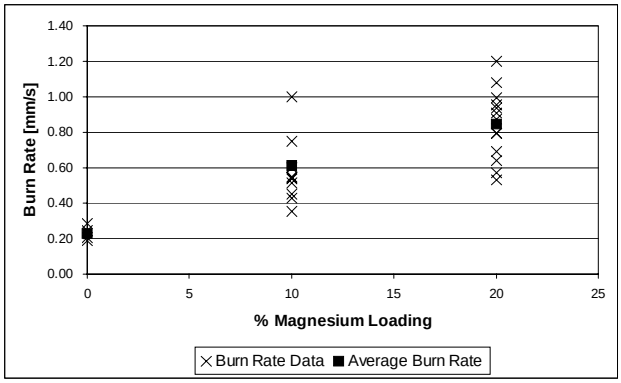

Figure 9. Burn-rate data. Magnesium loading of AN mixture. 20% HTPB, balance of mixture AN.

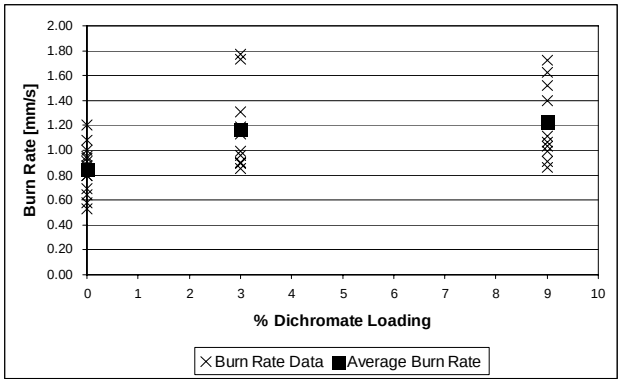

Figure 10. Burn-rate data. AD loading of AN mixture with Mg. 20% HTPB, 20% Mg, Balance of mixture AN.

Table 2. Comparison of average burn rates for AN-based solid fuels with HTPB or GAP

Mixture Ratio AN:Binder:Mg:AD	Average Burn Rates [mm/s]	
	HTPB	GAP
80:20:0:0	0.23	0.60
60:20:20:0	0.84	1.10
57:20:20:3	1.17	1.04

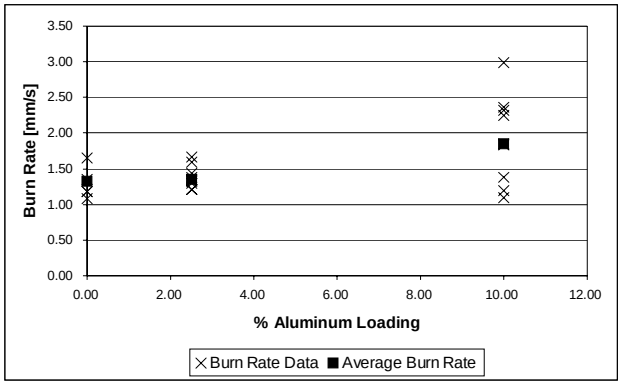

Figure 11. Burn-rate data. Aluminum loading of AP mixture. 20% HTPB, balance of mixture AP.

Table 3. Comparison of average burn rates for AP-based solid fuels with HTPB or GAP

Mixture Ratio AP:Binder:Al	Average Burn Rates [mm/s]	
	HTPB	GAP
80:20:0	1.32	1.57
70:20:10:0	1.84	1.68

AP-based fuels. In the next series of experiments, the AP-based fuel was modified to increase burn rate. First, in Fig. 11, aluminum metal fuel was added and observed to increase the burn rate from 1.32 mm/s to 1.84 mm/s with 10% Al added. In Table 3, the energetic GAP binder, increased burn rate from 1.32 mm/s to 1.57 mm/s when used only with AP. GAP produced a decrease in burn rate when combined with aluminum powder and AP; the burn rate decreased from 1.84 mm/s to 1.68 mm/s.

SA-based fuels. In the next series of experiments, SA-based fuel was modified to increase burn rate. First, in Fig. 12, the KNO3 was added and observed to increase the burn rate from 0.4 mm/s to 0.54 mm/s with 10% KNO3 added. An increase in KNO3 to 20% was observed to have no effect on burn rate. In Table 4, the energetic GAP binder, increased burn rate from 0.40 mm/s to 0.84 mm/s when used with SA. GAP also produced increases in burn rates when combined with KNO3 and SA; the burn rate increased from 0.54 mm/s to 1.07 mm/s.

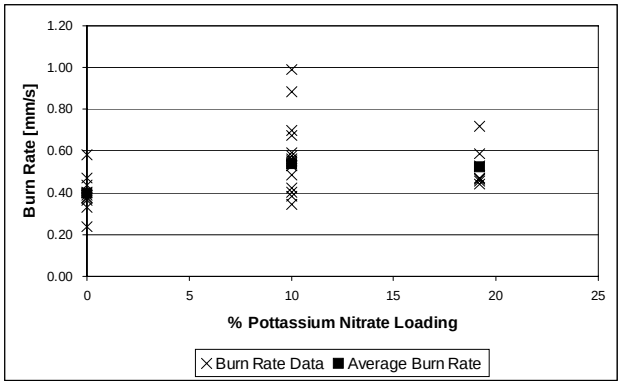

Figure 12. Burn rate data. KNO_3 loading of base SA mixture. 20% HTPB, balance of mixture SA.

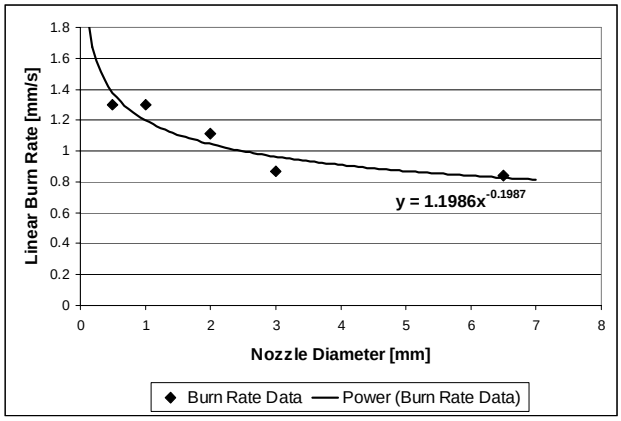

Figure 13. Burn rate data with nozzle. 3:1:1 Ratio of AN:HTPB:Mg

Table 4. Comparison of average burn rates for SA-based solid fuels with HTPB or GAP

Mixture Ratio SA:Binder:KNO_3	Average Burn Rates [mm/s]	
	HTPB	GAP
80:20:0	0.40	0.84
70:20:10:0	0.54	1.07
60:20:20	0.52	0.90

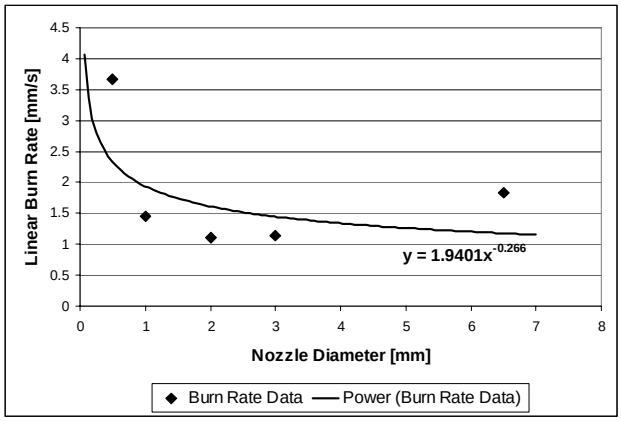

Figure 14. Burn rate data with nozzle. 7:2:1 Ratio of AP:HTPB:Al

Linear Burn Rate Testing with Nozzle

In the next series of experiments, nozzles are observed to increase average linear burn rates for the three base fuels. Figure 13 illustrates changes in burn rate with respect to nozzle diameter for a 3:1:1 ratio of AN:HTPB:Mg. For a 0.5 mm nozzle, linear burn rate for this mixture was measured to be 1.30 mm/s compared to 0.84 mm/s without a nozzle. Figure 14 shows changes in burn rate with respect to nozzle diameter for a 7:2:1 ratio of AP:HTPB:Al. For a 0.5 mm nozzle, linear burn rate for this mixture was measured to be 3.67 mm/s compared to 1.84 mm/s without a nozzle. Figure 15 shows changes in burn rate with respect to nozzle diameter for a 7:2:1 ratio of SA:HTPB:KNO_3. For a 0.5 mm nozzle, linear burn rate for this mixture was measured to be 5.21 mm/s compared to 0.54 mm/s without a nozzle.

Because burn rate is related to pressurization by Veille's law, a power curve has been fitted to the data in Figures 13 through 15. The trend lines relate linear burn rate to nozzle diameter by the following form:

$$r = cD^m$$

These experiments were also completed for similar formulations with GAP as a binder instead of HTPB. Rather than present these plots, Table 5 summarizes the power curve fit for the set of nozzle experiments.

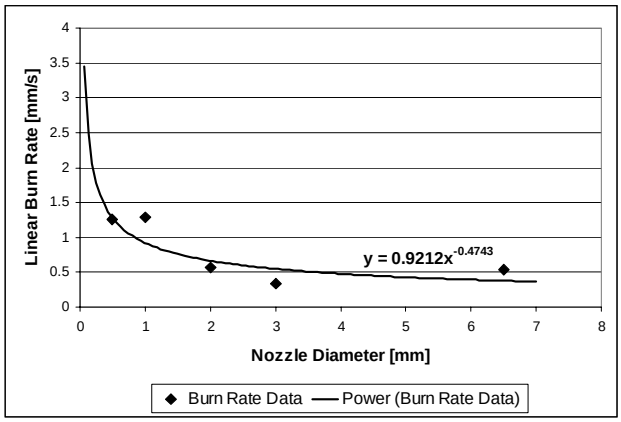

Figure 15. Burn rate data with nozzle. 7:2:1 Ratio of SA:HTPB:KNO_3

Table 5. Power fit coefficients for nozzle experiments

Fuel Composition	Binder			
	HTPB		GAP	
	c	m	c	m
3:1:1 AN:Binder:Mg	1.20	-0.20	1.25	-0.44
7:2:1 AP:Binder:Al	1.94	-0.27	1.85	-0.68
7:2:1 SA:Binder:KNO_3	0.92	-0.47	3.89	-0.92

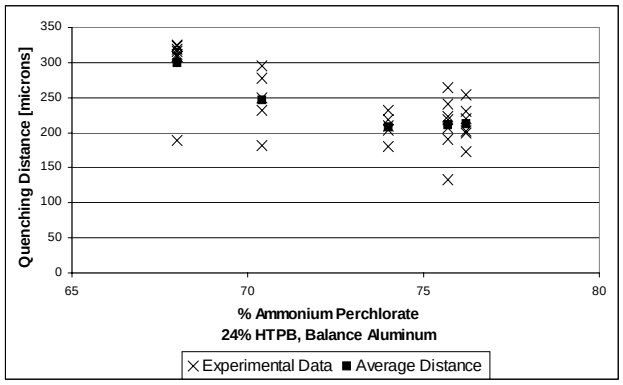

Figure 16. Quenching Data for AP-based solid fuel with HTPB binder

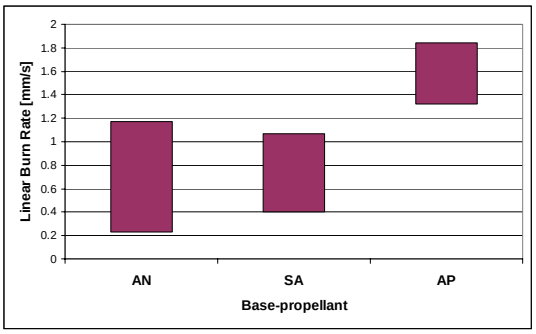

Figure 17. Base-fuel design space with various compositions

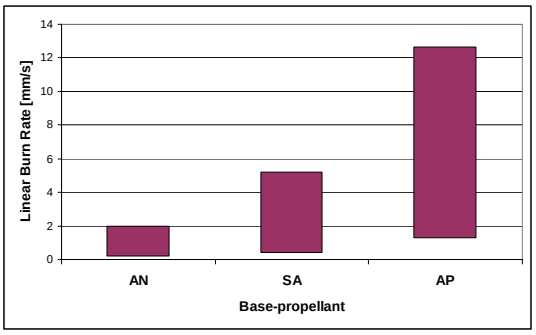

Figure 18. Solid-fuel design space including for various composition with nozzles.

Quenching Experiment Result

The next series of experiments attempt to terminate solid fuel combustion, specifically in AP-based fuels, by increasing heat loss to the combustion chamber. Figure 16 depicts quenching distance for several mixtures of AP-based solid fuel. The minimum quenching distance observed was 130 microns for a 75.7:24.3 AP:HTPB mixture. The minimum average quenching distance was calculated to be 210 microns for a 74:23.8:2.2 AP:HTPB:Al mixture. Higher concentrations of aluminum powder actually increases the average quenching distance from 210 microns to 300 microns; the mixture plotted on the left of Fig. 16 is 68:24:9 AP:HTPB:Al.

DISCUSSION

Control of solid-fuel burn rates has been demonstrated on the scale of hundreds of microns by three methods:

1- Changes in base composition and additives;
2- Pressurization due to a nozzle;
3- Increased heat losses to side walls.

The first method of control, changes in composition, demonstrates that choice of base fuel may be used to control linear burn rate and subsequent gas generation from a solid-fuel element. The choice of base fuel in a solid-fuel microactuator predetermines exhaust jet magnitude because the rate of gas production is directly proportional to the linear burn rate at the solid fuel surface. Also, if a single solid fuel element were to be consumed in a combustion event, the pulse duration of that event may be pre-designed based on the linear burn rate, by setting the characteristic combustion length of the solid-fuel elements. For example, if an element that burns at a rate of 1 mm/s will be consumed in 1/10 seconds, the characteristic burn length of that element should be 100 microns. The linear-burn-rate experiments predetermine a design space for the geometric placement of MEMS components in a solid fuel element. The base-fuel design space without nozzles and including the addition of additive tested in this study may be seen in Fig. 17.

The second method for controlling burn rate is the addition of a nozzle to provide additional heat and pressure-feedback to the reacting surface. The nozzle predictably raises the instantaneous pressure at the reacting surface, as implied by Veille's Law, so a power law fit was assumed for linear burn rate with respect to nozzle diameter. By varying nozzle diameter, an increase in design space was observed for the base solid fuel compositions. Figure 18 illustrates the increased range of burn rates which may be applied when designing controllable solid fuel elements for use in a solid-fuel microactuator. Comparing Fig. 18 to Fig. 17, the design space

increases by nearly 11 mm/s for AP, 4.8 for SA, and 1.77 for AN. Unlike in Fig. 17, Fig. 18 shows that SA does not fall within the design space of AN. This is most likely due to a greater solid-fuel to gas conversion rate for SA and due to increased combustion temperatures for SA compared with AN. The solid-fuel to gas conversion rates will have to be studied in the future to better predict actuator exhaust magnitude.

Finally, quenching tests demonstrated the ability to terminate a solid fuel reaction by increasing heat loss to side walls. This would conserve adjacent reactants for future combustion events. ON/OFF control of combustion events allows for increased control density when designing solid-fuel microactuators, because the chamber may be scaled to contain any combustion events to a specific region. Based on quenching results for a mixture of 4:1 AP:HTPB, a volume-to-surface ratio, or quenching distance, maintained below 212 microns would prevent combustion propagation throughout a chamber. This would further simplify MEMS fabrication of solid-fuel microcombustors because igniters may be tightly packed into a single combustion chamber, while the top and bottom of the chamber limit reaction propagation.

All three methods of solid-fuel control then may be used to control the pulse magnitude and pulse duration of a solid-fuel microactuator. The pulse duration may be limited by the solid-fuel element's characteristic burn length or by combustion-chamber quenching effects. The pulse magnitude may be controlled by choice of base fuel and by the addition of a nozzle. Combinations of many controllable solid fuel elements provide the basis for fabricating a controllable solid-fuel fluidic microactuator.

ACKNOWLEDGMENTS

This work was supported in part by the Defense Advanced Research Projects Agency Micro Adaptive Flow Control program. The authors would like to acknowledge Prof. Jerry Seitzman of Georgia Tech for valuable technical discussion.

REFERENCES

[1] Lewis Jr., D.H., Janson, S.W., Cohen, R.B., Antonsson, E.K., "Digital micropropulsion," *Sensors and Actuators A,* Volume 80, 2000, 143-154.

[2] Rossi, C., Estève, D., Mingués, C., "Prediction of performance of a Si-micromachined microthrusters by computing the subsonic gas flow inside the thruster," *Sensors and Actuators A*, Volume 87, 2000, pp. 96-104.

[3] Rossi, C., Mehdi Djafari Rouhani, Estève, D., "Pyrotechnic actuator: a new generation of Si integrated actuator," *Sensors and Actuators A*, Volume 74, 1999, pp. 211-215.

[4] Teasdale, D., "Solid Propellant Microrockets," Master's Thesis, Berkeley: University of California, 2000.

[5] Allen, M.G., and Glezer, A., "Alternative Micromachining Approaches for the Realization of Robust MEMS," American Institute of Aeronautics and Astronautics 38th Aerospace Sciences Meeting, Paper AIAA-2000-0248, January 2000.

[6] DeLuca, L.T., "Chapter 2: Burning Rate Fundamentals" [Online Document], 2001 Mar 27 (v01), available HTTP: http://www.energ.polimi.it/splab/pdf/DeLuca%20Chapter%202%20Web-01.pdf

[7] Sućeska, Muhammed, *Tests Methods for Explosives,* Springer-Verlag New York, 1995, p. 83.